Scientific paper

Zinc Metal-Organic Frameworks- Graphene Quantum Dots Nanocomposite Mediated Highly Sensitive and Selective Fluorescence "On-Off-On" Probe for Sensing of Quercetin

Sopan N. Nangare[1], Premnath M. Sangare[2], Ashwini G. Patil[3] and Pravin O. Patil[2,*]

[1] *Department of Pharmaceutics, H. R. Patel Institute of Pharmaceutical Education and Research, hirpur 425405, Dist: Dhule (MS), India.*

[2] *Department of Pharmaceutical Chemistry, H. R. Patel Institute of Pharmaceutical Education and Research, Shirpur 425405, Dist: Dhule (MS), India.*

[3] *Department of Microbiology, R. C. Patel Arts, Commerce and Science College, Shirpur 425405, Dist: Dhule (MS), India.*

* *Corresponding author: E-mail: rxpatilpravin@yahoo.co.in*

Received: 11-03-2022

Abstract

The current study presents a fluorescence-based 'On-Off-On' nanoprobe composed of rose petal-derived graphene quantum dots embedded in zinc metal-organic frameworks (RP-GQDs@Zn-MOFs) as a proof of concept for quercetin sensing. The particle size and HR-TEM analysis confirmed the synthesis of a uniformly distributed nanosized probe, while the zeta potential (+33.03 mV) verified its good stability. The fluorescence analysis confirmed that the introduction of copper ions (Cu^{2+}) resulted in fluorescence quenches, while the inclusion of quercetin forms quercetin-Cu^{2+} complex, leading to recovery of quenched fluorescence in RP-GQDs@Zn-MOFs due to static quenching. The nanoprobe demonstrated a wide concentration range and a low detection limit of 100 ng/mL to 1400 ng/mL ($R^2 = 0.99$) and 37.8 ng/mL, respectively. Selectivity analysis highlighted pronounced specificity for quercetin, attributed to Cu^{2+} coordination between carbonyl oxygen atom and the 3-OH group of quercetin. Furthermore, designed probe exhibited excellent stability, repeatability (RSD < 5), and potential for real-time analysis.

Keywords: Zinc metal-organic frameworks; graphene quantum dots; copper ions; quercetin; high sensitivity; high selectivity

1. Introduction

Metal-organic frameworks (MOFs) are preferred for various applications, including biomedical and environmental uses. This preference stems from their distinctive characteristics, such as their ability to modify surfaces, their large surface area, and their adjustable structure.[1] It provides a highly porous structure through the association of metal ions with carefully selected organic linkers via strong bonding.[2] To date, various types of MOFs have been developed for numerous applications, including drug delivery, biosensing, chemical sensing, gas separation, and more.[3,4] At present, they are widely employed for biosensing purposes, offering low detection limits, high sensitivity, excellent responsiveness, and good stability, among other benefits.[4] Despite these groundbreaking merits, MOFs suffer from major drawbacks, primarily the collapse of their structure and pore shrinkage.[2] As a result, there is a need for complementary nanoparticles that can help overcome these significant drawbacks while preserving the original features of MOFs.

Currently, significant efforts are underway to develop innovative MOFs-centered composites to address the genuine needs of the scientific community. Encapsulating nanosized components within MOFs represents a novel advancement in the biomedical field.[5,6] In this context, it is worth noting that fluorescence-mediated sensing tech-

niques are widely employed due to their several advantages, including a straightforward process, rapid detection, high sensitivity, and specificity compared to previously existing technologies.[7] Furthermore, MOFs are porous frameworks with numerous unsaturated metal coordination sites and superior surfaces, making them suitable hosts for the integration of fluorescent nanomaterials.[8] In this context, various types of fluorescent nanomaterials have been reported for the development of MOFs-based nanocomposites, including carbon dots,[9] graphene quantum dots (GQDs),[10] molybdenum disulfide quantum dots,[11] black phosphorus quantum dots,[12] and more. Among these, fluorescent GQDs have been extensively reported as the latest carbon-mediated nanomaterial for biomedical applications.[13] Interestingly, they offer good stability, consistent fluorescence, biocompatibility, and excellent aqueous solubility, among other qualities.[14] Furthermore, they have been widely favored for numerous biomedical applications, including drug delivery, biosensing,[15] and chemical sensing.[16] The bare, green-synthesized GQDs were used to detect curcumin.[17] In this case, the selective detection mechanism has been unknown. Additionally, it has been conjugated with various types of nanomaterials to achieve highly sensitive and selective recognition of the target analyte.[18,19] The designed nanoprobe based on GQDs and manganese dioxide nanosheets offers a simple, highly sensitive, and selective fluorescent 'Off-On' configuration.[20] In this situation, the primary focus was to maintain the sufficient fluorescence potential of GQDs and the substantial adsorption capacity of the functional material. Therefore, we aim to synthesize new RP-GQDs@Zn-MOFs nanoprobes by decorating RP-GQDs within Zn-MOFs.

Quercetin is a flavonoid primarily found in medicinal plants.[21] It plays a crucial role in accurate pharmacological response and monitoring of biochemical and biological activities.[22] Various recognition methods have been employed for the analysis of quercetin, including high-performance liquid chromatography,[23] fluorescence-centered sensing,[22] electroanalytical methods, and electrophoresis.[21] Despite the numerous advantages, there are several drawbacks, including the cost factor, and the need for larger equipment, expertise, and solvents. Furthermore, there is a desire to enhance the sensor's sensitivity and selectivity.

In this study, our objective was to design a new RP-GQDs@Zn-MOFs fluorescence-based sensor through a simple method and demonstrate its utility in sensing quercetin as a proof of concept. In brief, this work involved synthesizing Zn-MOFs using zinc ions (Zn^{2+}) as the metal source and 2-methyl-1*H*-imidazole as an organic linker. Simultaneously, we focused on synthesizing RP-GQDs using rose petal waste. By combining the desirable fluorescence potential of RP-GQDs and the substantial adsorption capability of Zn-MOFs, we aimed to create new RP-GQDs@Zn-MOFs nanoprobes through the incorporation of RP-GQDs onto Zn-MOFs. To enhance selectivity for the target analyte, we developed a quenched version of the Cu^{2+}-RP-GQDs@Zn-MOFs probe, utilizing copper ions (Cu^{2+}) to confer specificity. Ultimately, our research aimed to evaluate the performance of the quenched Cu^{2+}-RP-GQDs@Zn-MOFs probe, prepared by combining RP-GQDs and Zn-MOFs, for the sensitive, specific, simple, rapid, and cost-effective detection.

2. Materials and Methods

2. 1. Materials

Rose petal waste was collected from a local market in Shirpur, Maharashtra, India. Zinc dinitrate hexahydrate (molecular formula: $H_{12}N_2O_{12}Zn$), and 2-methyl-1*H*-imidazole (molecular formula: $C_4H_6N_2$) were purchased from Loba Chemie Pvt. Ltd., Mumbai, India. Copper dinitrate was purchased from Sigma-Aldrich Chemicals Pvt. Ltd., Bangalore, India. Sodium hydroxide (NaOH) was supplied from Merck Specialties Pvt. Ltd., Mumbai, India. Methanol was purchased from Loba Chemie Pvt. Ltd., Mumbai, India. Sulphuric acid was purchased from Merck Specialties Pvt. Ltd., Mumbai, India. Quercetin was obtained from Otto Chemicals in Marine Lines, Mumbai, India. Ethanol was purchased from Anil Cottage Industries, A/31, M.I.D.C., Wardha, India. Also, the HPLC grade deionized water (DI, 0.2 μm filtered) and hydrochloric acid (HCl) were purchased from Avantor Performance Materials India Ltd., Thane, India. Quinine sulfate (99%) was purchased from Loba Chemie Pvt. Ltd., Mumbai, India. Phosphate buffer tablets (pH 7.4) were obtained from Loba Chemie Pvt. Ltd., Mumbai, India. All chemicals employed in the research study were analytical grade and pure, as supplied by the distributor.

2. 2. Methods

2. 2. 1. Synthesis of RP-GQDs using the Green Approach

At the outset, abandoned rose petals were acquired from a local market and cut into small fragments before being ground into a paste using a mortar and pestle. The creation of RP-GQDs from these discarded rose petals was achieved using a one-pot hydrothermal technique. To summarize, 10 g of the rose petal paste was homogenized with 50 mL of distilled water (DI water) and sonicated for 20 min. The resulting dispersion was then transferred into a Teflon-lined autoclave and heated for 10 h at 200 °C. After the reaction, the slurry was cooled to room temperature. To obtain a uniform dispersion, the resulting dark brown dispersion was ultrasonicated for 10 min. Subsequently, the dispersion was passed through a 0.22 μm microporous membrane to remove any insoluble or untreated carbonous elements. The resulting filtrate was retained for 36 h and subjected to rinsing using a dialysis bag (12,000 kDa). Afterwards, the outer dispersion was collected and

processed in a hot air oven (Bio-Technics, India) at 60 °C for 24 h.[4] Finally, the photoluminescence spectrum analysis of the obtained RP-GQDs was conducted.

2. 2. 2. Synthesis of Zn-MOFs

We adopted the previously published strategy for the fabrication of Zn-MOFs.[24,25] To begin, 2 g of zinc dinitrate hexahydrate (as the source of metal ions) was evenly mixed in 10 mL of distilled water (DI water) at 50 rpm. Simultaneously, at room temperature, 4 g of 2-methyl-1*H*-imidazole (the organic linker) was dissolved in 10 mL of DI water. The zinc solution was then combined with the 2-methyl-1*H*-imidazole solution while continuously stirring at 100 rpm. All procedures were carried out at 20 °C. Subsequently, a milky precipitate formed, indicating the formation of Zn-MOFs. Afterwards, the Zn-MOFs precipitate was centrifuged and washed three times with DI water. Finally, the drying of Zn-MOFs was achieved using a laboratory hot air oven (Bio-Technics, India) at 60 °C. The photoluminescence spectra of the resulting Zn-MOFs were then analyzed.

2. 2. 3. Development of RP-GQDs@Zn-MOFs

In this phase, we employed various diluted concentrations of Zn-MOFs to assess the impact on the strong fluorescence of RP-GQDs. Fluorescence spectra of RP-GQDs were recorded using an excitation wavelength of 330 nm. Subsequently, 10 ppm solutions of Zn-MOFs in phosphate-buffered saline (PBS) at pH 7.4 were prepared for the fabrication of the RP-GQDs@Zn-MOFs probe. Different concentrations of Zn-MOFs were individually added to 1.5 mL of RP-GQDs to optimize the overall fluorescence of the probe. The fluorescence change of RP-GQDs was assessed after 5 min. Finally, the concentration of Zn-MOFs used for constructing the RP-GQDs@Zn-MOFs fluorescence nanoprobe was determined. For this purpose, a physical absorption technique was employed to synthesize the RP-GQDs@Zn-MOFs probe. Specifically, 1.5 mL of RP-GQDs and 0.5 mL of pre-synthesized Zn-MOFs (10 ppm) were combined and magnetically stirred for 15 min. To separate the nanoconjugates, the resulting mixture was centrifuged at 15,000 rpm for 45 min using a refrigerated centrifuge (Eltek Overseas Pvt., India), and then washed four times with ethanol to remove unreacted species. To examine the variation in fluorescence intensity, we conducted a photoluminescence spectrum analysis of the resulting RP-GQDs@Zn-MOFs probe.

2. 2. 4. Spectroscopical Characterization

Ultraviolet-visible (UV-Vis) spectroscopy was employed to confirm the synthesis of RP-GQDs, Zn-MOFs, and RP-GQDs@Zn-MOFs using a UV-Vis Spectrophotometer (UV 1800 Shimadzu, Japan) with a scanning wavelength range of 200 nm to 800 nm, utilizing a quartz cuvette (1 cm). The fluorescence behavior of RP-GQDs, Zn-MOFs, and RP-GQDs@Zn-MOFs was observed within a laboratory UV cabinet (Southern Scientific Lab Instruments, Chennai, India) under different lighting conditions, including visible light, short UV (wavelength: 254 nm), and long UV (wavelength: 365 nm). Excitation spectra, emission spectra, and sensing were performed using a Jasco fluorescence spectrophotometer (FP-8200). Subsequently, Fourier transform infrared spectroscopy (FTIR, IR-Affinity-1, Shimadzu) was utilized to investigate the surface functionality of the synthesized RP-GQDs, Zn-MOFs, and RP-GQDs@Zn-MOFs over a scanning wavelength range from 400 cm^{-1} to 4000 cm^{-1}. Particle size, polydispersity index, and zeta potential analysis were conducted using a Particle size analyzer (Nanoplus 3, Micromeritics, USA). The powder X-ray diffraction (PXRD) analysis of RP-GQDs, Zn-MOFs, and RP-GQDs@Zn-MOFs was conducted using an X-ray diffractometer (D2 PHASER). The dimensions and selected area diffraction (SAED) pattern of RP-GQDs, Zn-MOFs, and RP-GQDs@Zn-MOFs were confirmed through high-resolution transmission electron microscopy (HR-TEM-SAED, Jeol/JEM 2100) utilizing a LaB6 light source at 200kV (STIC Cochin, India).

2. 2. 5. Fluorescence Study and Quantum Yield (% QY)

In this case, we measured the fluorescence intensity of the synthesized RP-GQDs, Zn-MOFs, and RP-GQDs@Zn-MOFs probe using a spectrofluorometer (JASCO FP 8200 Spectrofluorometer). Additionally, we assessed the excitation-emission spectrum of the produced RP-GQDs, as well as the photoluminescence behavior of the RP-GQDs at different excitation wavelengths ranging from 300 nm to 350 nm. Following these measurements, we determined the % QY (quantum yield) of RP-GQDs using the previously reported method.[4] In brief, quinine sulfate (with a known quantum yield, QY = 0.54, in 0.1 M sulfuric acid) served as the reference standard. Simultaneously, RP-GQDs were dissolved in deionized (DI) water, and their concentrations were adjusted to achieve a UV absorbance value of less than 0.1. For the analysis, a 10 mm cuvette was utilized, and slit widths were set at 5 nm for both excitation and emission. Finally, the fluorescence emission spectra of the standard and RP-GQDs were measured at an excitation wavelength of 330 nm. The following formula (1) was employed for calculating the % QY.

$$QYs = QYr\frac{I(Ar)ns^2}{Ir(As)nr^2} \quad (1)$$

Wherein, 'QYs' and 'QYr' represent the quantum yields of the sample and the standard reference, respectively. Similarly, 'Is' and 'Ir' denote the unified photoluminescence intensities of the sample and the reference standard. 'Ar' and 'As' correspond to the absorbance values, while

'nr' and 'ns' signify the refractive indices of the reference and the sample, respectively.

2. 2. 6. Sensing of Quercetin

In this study, we measured the changes in fluorescence of RP-GQDs, Zn-MOFs, and RP-GQDs@Zn-MOFs using a spectrofluorometer. Subsequently, we executed the detection of quercetin using a fluorescent RP-GQDs@Zn-MOFs probe. In essence, we prepared a stock solution of 5 mg of quercetin (50 μg/mL) by dissolving it in a volumetric flask containing 100 mL of deionized (DI) water (at 18 °C). Using this stock solution, we created different concentrations of quercetin, ranging from 100 ng/mL, 200 ng/mL, 300 ng/mL, 400 ng/mL, 500 ng/mL, 600 ng/mL, 700 ng/mL, 800 ng/mL, 900 ng/mL, 1000 ng/mL, 1100 ng/mL, 1200 ng/mL, 1300 ng/mL and 1400 ng/mL in cleaned volumetric flasks (n = 3). Meanwhile, we dissolved 10 mg of RP-GQDs@Zn-MOFs fluorescent probe in 100 mL of DI water. Next, we assessed the fluorescence intensity of the designed probe at an excitation wavelength of 330 nm (n = 3). For this work, we adopted the Cu^{2+}-Zn-MOFs@RP-GQDs probe as a new sensory platform. In this case, we evaluated different concentrations of Cu^{2+} (ranging from 0.1 mL, 0.2 mL, 0.3 mL, 0.4 mL, 0.5 mL, 0.6 mL, 0.7 mL, 0.8 mL, 0.9 mL, 1.0 mL, 1.1 mL, and 1.2 mL of a 0.16 mM Cu^{2+} solution) as quenching agents to suppress the fluorescent ability of the Zn-MOFs@RP-GQDs, leading to a fluorescent "Turn-Off" effect (n = 3). Following this, the concentration of Cu^{2+} ions at which the RP-GQDs@Zn-MOFs probe fluorescence was completely quenched was considered the optimized concentration of Cu^{2+} ions. Subsequently, several RP-GQDs@Zn-MOFs probes were designed as a sensory platform for the recognition of quercetin, with fluorescence quenching being ensured for each probe, separately (n = 3). In brief, the probes were prepared in individual test tubes containing 1.2 mL of a 0.16 mM Cu^{2+} ion solution and left for 5 min at 25 °C. The first probe was then incubated with a 100 ng/mL concentration of quercetin to initiate complex formation between Cu^{2+} ions and quercetin. In this step, the recovery of the quenched fluorescence of RP-GQDs@Zn-MOFs referred to as "Turn-On," was monitored. The fluorescence intensity was measured using optimized parameters at an excitation wavelength of 330 nm. The same procedure was applied to the other prepared quercetin concentrations (samples), each time with a fresh Cu^{2+}-RP-GQDs@Zn-MOFs probe. Each experiment was performed in triplicate to confirm their reproducibility. Finally, the linear concentration range was determined by plotting the recovered probe fluorescence against quercetin concentration. Additionally, the limit of detection (LOD) and limit of quantification (LOQ) were computed using previously described methods and formulas (2) and (3).

$$\text{LOD: } 3.3^{*}\sigma/m \quad (2)$$

$$\text{LOQ: } 10^{*}\sigma/m \quad (3)$$

In this context, 'm' (slope) and 'σ' (standard deviation) were obtained from the calibration curve of quercetin concentration (ng/mL) *vs.* the recovery of fluorescent intensity of the quenched RP-GQDs@Zn-MOFs probe.

Stability and repeatability are crucial parameters for this sensor. Therefore, the stability of the envisioned RP-GQDs@Zn-MOFs fluorescent probes was assessed. Specifically, the concentration of quercetin at 600 ng/mL for six consecutive days was recorded using a manufactured probe (n = 6) under laboratory-programmed parameters at 25 °C. Subsequently, the efficiency of the sensory system was evaluated and computed the percent relative standard deviation (% RSD). Furthermore, the repeatability of the probe for the detection of quercetin was investigated using the RP-GQDs@Zn-MOFs probe (n = 9), with quercetin concentrations set at 500 ng/mL for assessment. Finally, the percentage RSD was calculated based on the collected responses.

2. 2. 7. Interference Study and Spiked Sample Analysis

In this study, plasma served as the representative sample. In brief, the various potential interfering agents were selected based on the composition of plasma to evaluate the selectivity of the designed RP-GQDs@Zn-MOFs fluorescence probe. Additionally, other interfering agents were randomly chosen for confirmation. In summary, we tested the selectivity of the RP-GQDs@Zn-MOFs fluorescence probe towards quercetin in the presence of several interfering chemicals, including ascorbic acid, glucose, albumin, potassium (K^{+}), magnesium (Mg^{2+}), calcium (Ca^{2+}), sodium (Na^{+}), citric acid, ascorbic acid, glycine, and others. To do this, 2 mL of the Cu^{2+}-RP-GQDs@Zn-MOFs probe was incubated with 600 ng/mL of quercetin, while different interfering elements (600 ng/mL) were introduced separately to the Cu^{2+}-RP-GQDs@Zn-MOFs probe in individual test tubes. The concentration of interfering agents remained constant to assess their effects at the same concentration as quercetin. Subsequently, we evaluated the fluorescence intensity for each sample using preprogrammed settings. Also, spiked sample analysis of quercetin in artificial plasma was performed using the Cu^{2+}-RP-GQDs@Zn-MOFs probe. In this procedure, an artificial plasma sample was prepared using a previously described method.[26] Afterwards, 1000 ng/mL of quercetin was added into a test tube containing 1 mL of artificial plasma sample (n = 3). Simultaneously, a placebo test tube containing only 1 mL of artificial plasma sample was prepared. Then the 500 ng/mL quercetin-containing plasma sample was added to 2 mL of Cu^{2+}-RP-GQDs@Zn-MOFs probe. The test tube was allowed to sit for 5 min, after which the fluorescence intensity of the Cu^{2+}-RP-GQDs@Zn-MOFs probe was monitored under optimized conditions. Finally, the percent recovery of quercetin and %

RSD was calculated to confirm the real-time applicability of the proposed Cu^{2+}-RP-GQDs@Zn-MOFs probe.

3. Results and Discussion

3. 1. UV Cabinet Fluorescence Study

RP-GQDs were initially synthesized from rose petal waste using a hydrothermal technique in a stainless steel Teflon line reactor. Subsequently, the resulting RP-GQDs were analyzed for fluorescence within a UV cabinet. RP-GQDs exhibited a yellow color under visible light (Figure 1A), greenish fluorescence when excited with 254 nm light (Figure 1B), and blue fluorescence when excited with 365 nm light (Figure 1C). This observation supported the successful synthesis of carbon-centered RP-GQDs from rose petal waste. Furthermore, the fluorescence capacity of the Zn-MOFs diminished under various UV lights, indicating that Zn-MOFs lacked fluorescence capabilities. However, the final product of the RP-GQDs@Zn-MOFs probe exhibited fluorescence properties similar to RP-GQDs (Figure 1D). The presence of blue fluorescence under UV light with an excitation wavelength of 365 nm in RP-GQDs@Zn-MOFs confirmed the successful encapsulation of RP-GQDs within Zn-MOFs without compromising the fluorescence behavior of RP-GQDs.

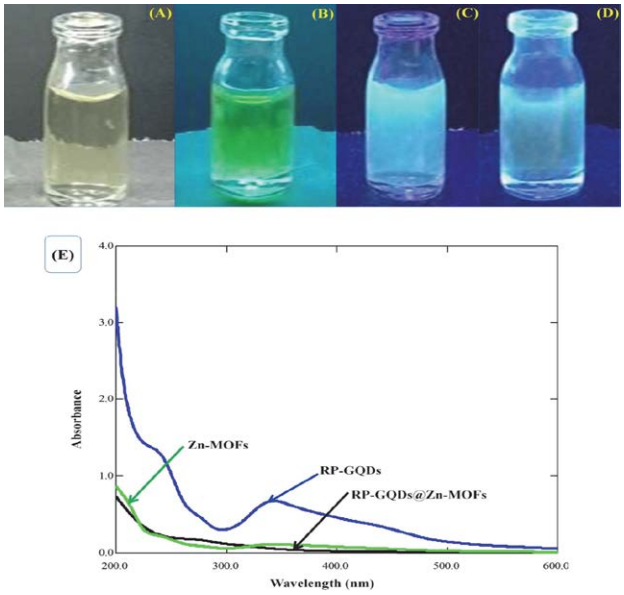

Figure 1: Photographs of RP-GQDs under visible light (A), UV light with λ_{Ex} 254 nm (B), and λ_{Ex} 365 nm (C) taken inside a UV cabinet. (D) Photographs of the RP-GQDs@Zn-MOFs probe under UV light with λ_{Ex} 365 nm in the UV cabinet. (E) UV spectral analysis of RP-GQDs, Zn-MOFs, and the RP-GQDs@Zn-MOFs probe.

3. 2. UV Vis Spectroscopy

The UV-Vis spectra of RP-GQDs, Zn-MOFs, and RP-GQDs@Zn-MOFs are presented in Figure 1E. In these spectra, RP-GQDs exhibit a prominent absorption peak ranging from 238 nm to 341.50 nm, which supports the $\pi \rightarrow \pi^*$ transition of sp^2 C=O bonds and the $n \rightarrow \pi^*$ transition of C=O bonds, respectively.[27] This observation suggests that RP-GQDs are derived from rose petal waste and possess carboxylic functionality on the surface of RP-GQDs. The UV-Vis absorption spectra of Zn-MOFs exhibit a peak at 239 nm, confirming the successful synthesis of Zn-MOFs, which is consistent with previously reported literature.[24] The final composite, RP-GQDs@Zn-MOFs, displays a broadened absorption spectrum. In this case, the absorption peak intensities of both RP-GQDs and Zn-MOFs were observed to decrease, possibly indicating efficient encapsulation of RP-GQDs within the Zn-MOFs structure.[25] Ultimately, this confirms the successful fabrication of RP-GQDs utilizing Zn-MOFs as a fluorescent detector for precise target measurements as a proof of concept.

3. 3. Fluorescence Study and % QY Measurement

The excitation and emission spectra of RP-GQDs were measured using a spectrofluorometer at various excitation wavelengths ranging from 290 nm to 360 nm under controlled experimental conditions, including a temperature of 25 °C. The photoluminescence ability of green-synthesized RP-GQDs, dependent on excitation wavelength (ranging from 310 nm to 350 nm), is illustrated in Figure 2A. Initially, excitation wavelengths from 310 nm to 330 nm resulted in a shift of the emission peak towards longer wavelengths (from 429 nm to 492 nm). Additionally, there was an increase in emission peak intensity up to an excitation wavelength of 330 nm. Surprisingly, a strong emission peak at 492 nm was observed with an excitation wavelength of 330 nm. Furthermore, as the excitation wavelength increased, the peak emission intensity decreased from 340 nm to 350 nm. Overall, the photoluminescence of the obtained RP-GQDs was found to be dependent on the excitation wavelength. In this study, the excitation and emission spectra for green-processed GQDs were reported at 288 nm and 492 nm, respectively (Figure 2B). Subsequently, RP-GQD QY were calculated to be 18.20%. In conclusion, the excellent optical properties of RP-GQDs synthesized using the green method were confirmed. Figure 2C depicts a comparison of the fluorescence behavior of RP-GQDs, Zn-MOFs, and RP-GQDs@Zn-MOFs. In this case, Zn-MOFs displayed the absence of fluorescence. Conversely, the obtained RP-GQDs exhibited strong fluorescence at 492 nm. Importantly, the conjugation of Zn-MOFs and RP-GQDs did not significantly alter the fluorescence behavior of RP-GQDs. Hence, it validates the development of the fluorescence-based RP-GQDs@Zn-MOFs probe.

3. 4. FT-IR Spectroscopy

Figure 3 displays the FT-IR spectrum of RP-GQDs, Zn-MOFs, and RP-GQDs@Zn-MOFs. In this case, the use

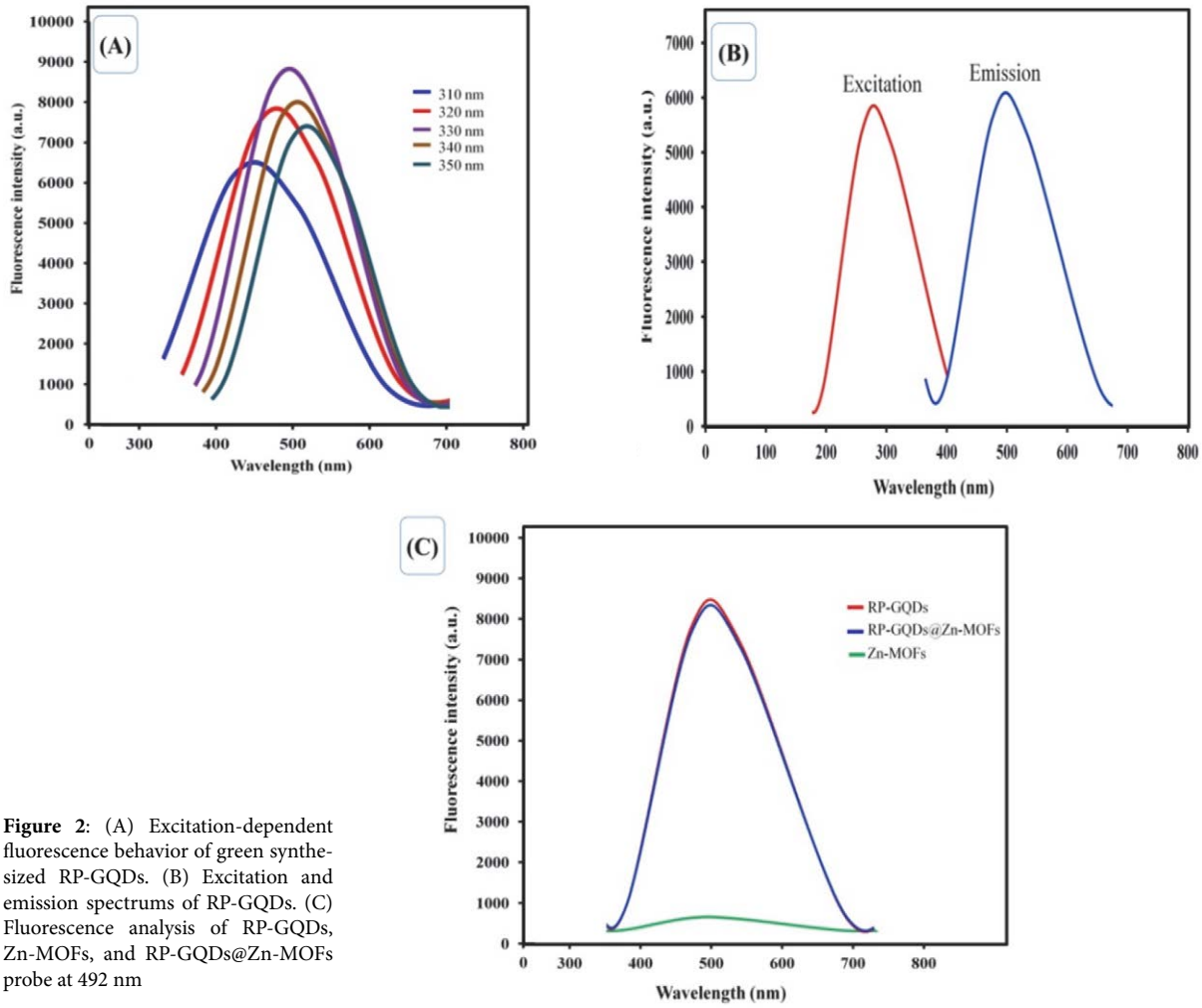

Figure 2: (A) Excitation-dependent fluorescence behavior of green synthesized RP-GQDs. (B) Excitation and emission spectrums of RP-GQDs. (C) Fluorescence analysis of RP-GQDs, Zn-MOFs, and RP-GQDs@Zn-MOFs probe at 492 nm

of FT-IR for RP-GQDs and Zn-MOFs aids in the characterization of the RP-GQDs@Zn-MOFs probe. The FT-IR spectrum of RP-GQDs exhibits peaks at 3403.57 cm^{-1}, 1637.6 cm^{-1}, and 1079.14 cm^{-1}, respectively, indicating the presence of -OH, C=O, and C-O functionalities.[28] This confirms the presence of hydroxylic and carboxylic functionality in RP-GQDs, ensuring good solubility in water. The FT-IR spectrum of Zn-MOFs shows peaks at 2931 cm^{-1} and 2864 cm^{-1}, verifying the presence of the C–H stretching mode of the aromatic ring and aliphatic chain present in 2-methyl-1*H*-imidazole. Additionally, the peaks at 1089 cm^{-1} and 1434 cm^{-1} confirm the presence of imidazole ring-related stretching and bending modes. Finally, the peak at 1600 cm^{-1} assures the existence of the C-N stretching mode in 2-methyl-1*H*-imidazole, while the broad peak at 3220 cm^{-1} verifies the presence of -OH stretching in Zn-MOFs, which may be due to the presence of water content. In the case of the RP-GQDs@Zn-MOFs probe, the peak at 3312 cm^{-1} confirms the presence of OH stretching in RP-GQDs, while the peaks at 2931 cm^{-1} and 2864 cm^{-1} verify the presence of the C–H stretching mode of the aromatic ring and aliphatic chain present in the linker of Zn-MOFs. Additionally, the peaks at 1664 cm^{-1} and 1093 cm^{-1} indicate the presence of C=O and C-O stretching, which are characteristics of RP-GQDs, while the peak

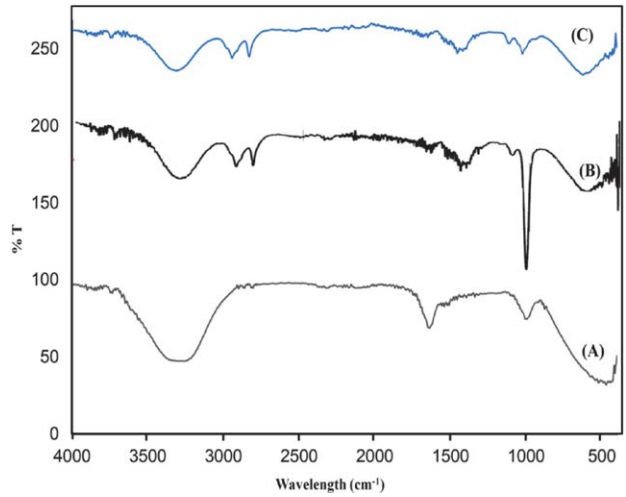

Figure 3: FTIR of (A) RP-GQDs, (B) Zn-MOFs, and (C) RP-GQDs@Zn-MOFs probe

at 1584 cm^{-1} assures the presence of the C-N stretching mode in 2-methyl-1*H*-imidazole. Therefore, this confirms the formation of RP-GQDs embedded in Zn-MOFs, constituting the RP-GQDs@Zn-MOFs probe.

3. 4. Particle Size and Zeta Potential Analysis

Figure 4 presents the particle size distribution of RP-GQDs, Zn-MOFs, and the RP-GQDs@Zn-MOFs probe. To summarize, the particle size of the obtained RP-GQDs was estimated to be 10.80 nm, and the polydispersity index (PDI) was found to be 0.32. This confirms the production of nanosized GQDs in water with a uniform distribution in the system. In Figure 4B, the particle size of Zn-MOFs is represented, with the average diameter and PDI confirmed as 141.20 nm and 0.26, respectively. The average diameter and PDI of the final RP-GQDs@Zn-MOFs probe were observed to be 158.23 nm and 0.36, respectively. HR-TEM analysis was conducted to verify the precise dimensions of RP-GQDs, Zn-MOFs, and the RP-GQDs@Zn-MOFs probe. Zeta potential analysis was performed to assess stability. Figure 5 illustrates the zeta potential analysis of RP-GQDs, Zn-MOFs, and the RP-GQDs@Zn-MOFs probe. Due to the presence of oxygen functionality on the surface of RP-GQDs, the zeta potential was confirmed to be –14.82 mV, indicating excellent stability of nanosized RP-GQDs in an aqueous environment and the potential for interaction with Zn^{2+} ions from Zn-MOFs.[29] As a result of Zn^{2+} ions, the zeta potential of Zn-MOFs was confirmed to be +41.32 mV. Finally, the zeta potential of the RP-GQDs@Zn-MOFs probe was reported to be +33.03 mV, lower than that of the naked Zn-MOFs in this study, possibly due to interactions between Zn-MOFs and RP-GQDs. In conclusion, this confirms the construction of a stable form of RP-GQDs, Zn-MOFs, and the RP-GQDs@Zn-MOFs probe.

3. 5. PXRD Analysis

Figure 6 represents the diffractogram of RP-GQDs, Zn-MOFs, and the RP-GQDs@Zn-MOFs probe. In brief, the diffractogram of RP-GQDs shows a sharp diffraction peak at 2θ = 10.59°, 12.83°, 14.84°, 16.73°, 18.12°, 24.75°, 26.74°, 29.92°, 35.08°, 36.65°, etc. confirming that the ob-

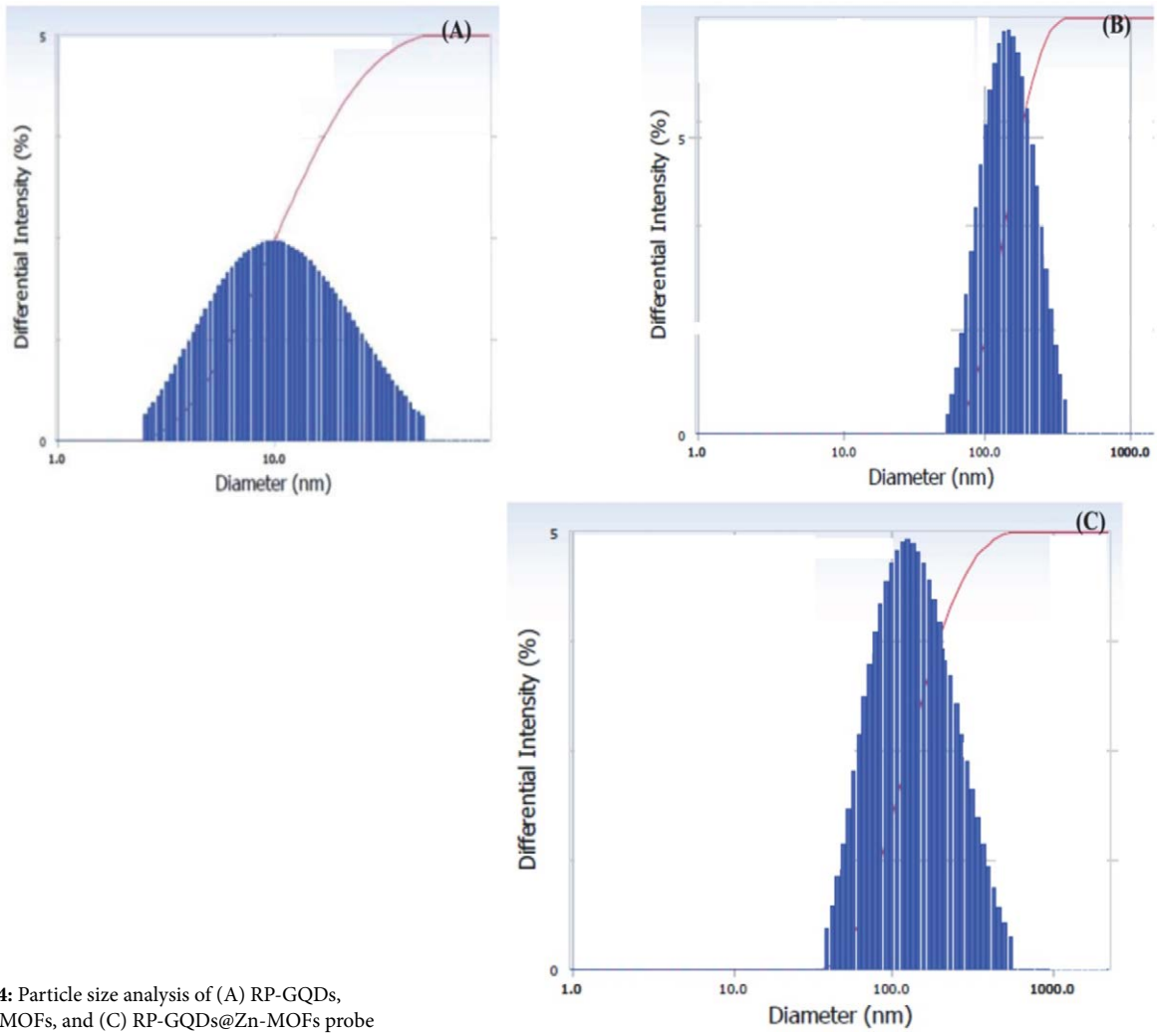

Figure 4: Particle size analysis of (A) RP-GQDs, (B) Zn-MOFs, and (C) RP-GQDs@Zn-MOFs probe

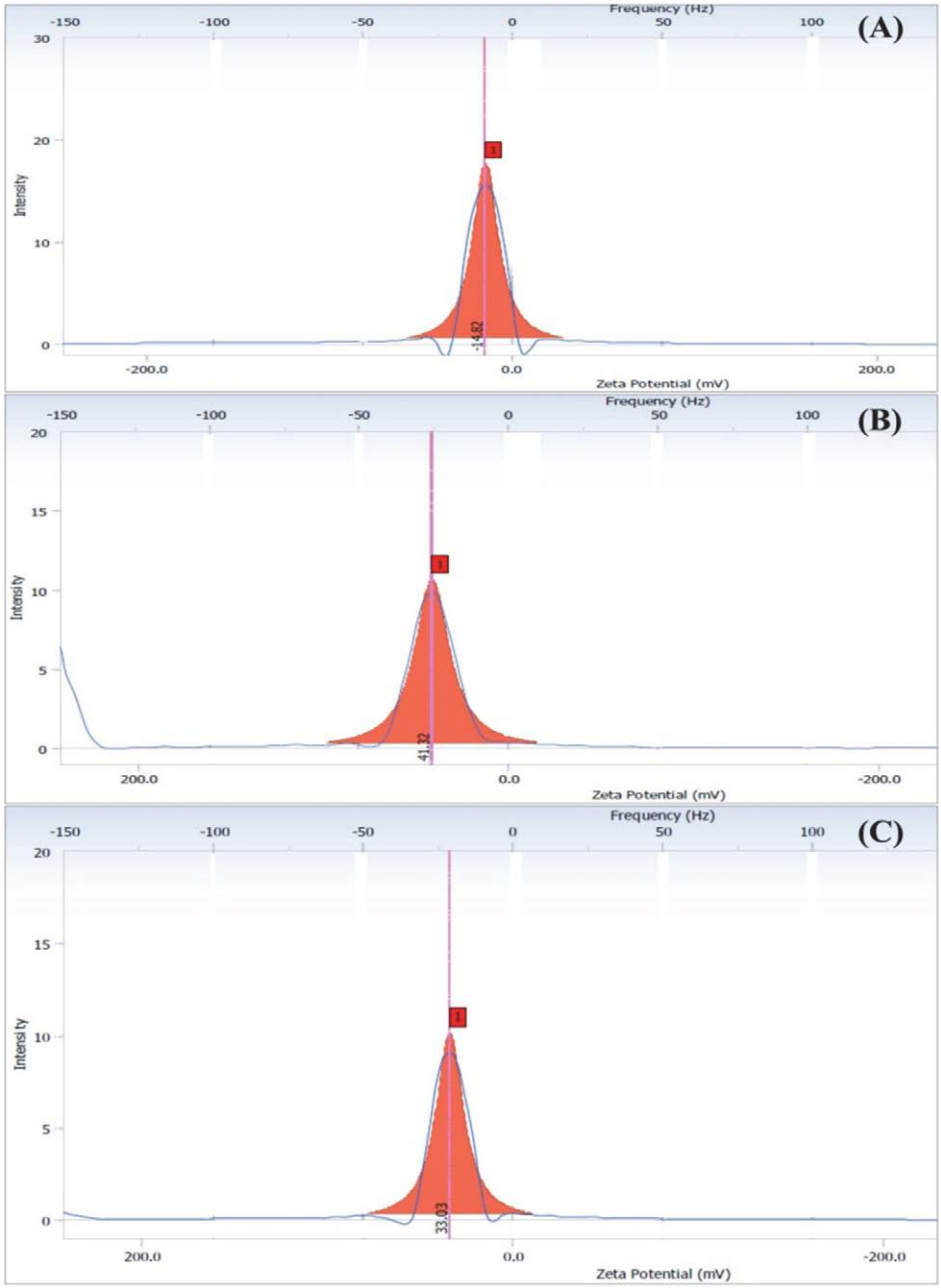

Figure 5: Zeta analysis behavior of (A) RP-GQDs, (B) Zn-MOFs, and (C) RP-GQDs@Zn-MOFs probe

tained RP-GQDs are highly crystalline. Similarly, both the Zn-MOFs and RP-GQDs@Zn-MOFs probe exhibit sharp diffraction peaks at 2θ = 10.47°, 13.23°, 16.75°, 18.24°, 21.20°, 23.58°, 25.35°, 26.56°, 28.43°, 30.57°, 33.89°, and 36.54° confirming the formation of a crystalline form of Zn-MOFs in both cases. Furthermore, the diffractogram of the RP-GQDs@Zn-MOFs probe only shows characteristic peaks of Zn-MOFs, with no discernible peaks from RP-GQDs.[30] It is possible that the incorporation of RP-GQDs into the framework of Zn-MOFs, where the surface carboxylic functionality of RP-GQDs may interact with the amine functionality of 2-methyl-1*H*-imidazole (the organic linker).[31] Additionally, the fact that there was no change in the diffractogram of Zn-MOFs after conjugation with RP-GQDs confirms the probe stability.

3. 6. HR-TEM Analysis

Figure 7 presents the HR-TEM images and SAED patterns of RP-GQDs, Zn-MOFs, and the RP-GQDs@Zn-MOFs probe. In essence, RP-GQDs were found to exhibit a spherical shape with a uniform distribution. The average diameter of RP-GQDs was measured to be 8.68 nm,

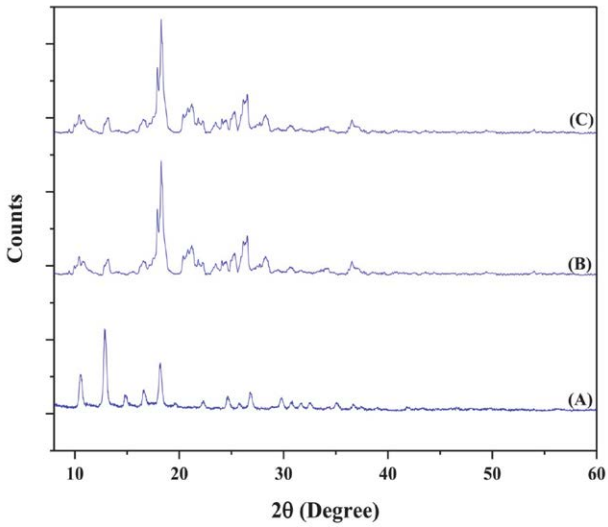

Figure 6: Diffractogram of (A) RP-GQDs, (B) Zn-MOFs, and (C) RP-GQDs@Zn-MOFs probe

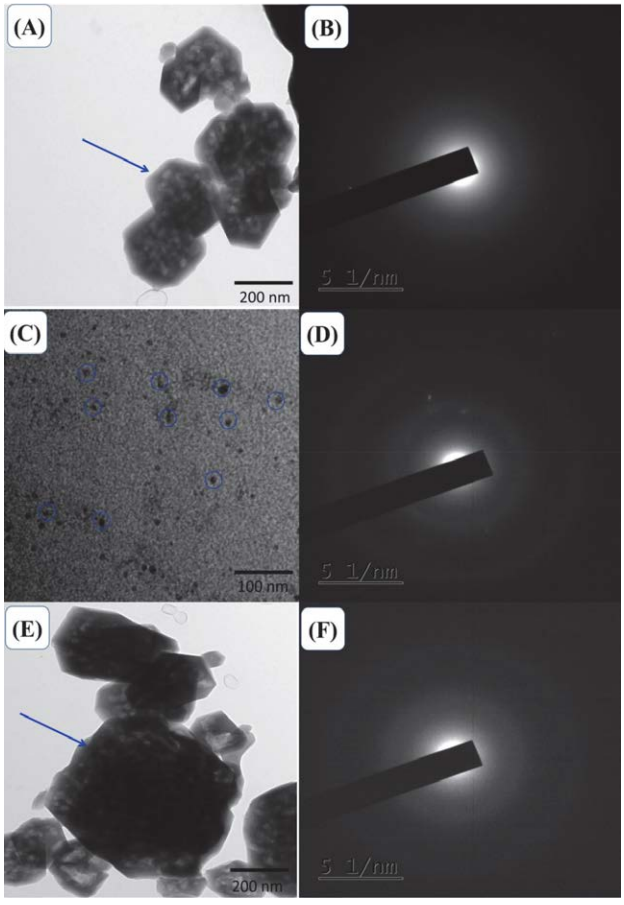

Figure 7: HR-TEM images and SAED pattern of (A, B) RP-GQDs, (C, D) Zn-MOFs, and (E, F) RP-GQDs@Zn-MOFs probe, respectively

confirming the synthesis of nanoscale GQDs from a green precursor. The HR-TEM image of Zn-MOFs displayed a hexagonal form, with an average diameter of 210.12 nm.[32] The surface morphology of the RP-GQDs@Zn-MOFs probe closely resembles that of the Zn-MOFs, with an average diameter of 226.98 nm. This observation is crucial as it confirms the successful assembly of the RP-GQDs@Zn-MOFs probe without any disruption of the Zn-MOF frameworks. Finally, the selected area electron diffraction (SAED) patterns of Zn-MOFs, RP-GQDs, and the RP-GQDs@Zn-MOFs probe indicate their polycrystalline nature.

3. 7. Sensing of Quercetin

To detect quercetin, a stable and nanosized RP-GQDs@Zn-MOFs probe was created, wherein zinc (Zn^{2+}) ions and carboxylic ions engage in a charge-charge interaction, effectively linking the RP-GQDs and Zn-MOFs. Additionally, hydrogen bonding interactions involving RP-GQDs with carboxyl, epoxy, and hydroxyl groups, as well as Zn-MOFs with amine functionality of 2-methyl-1*H*-imidazole, contribute to the formation of the RP-GQDs@Zn-MOFs probe (Turn-On). In this configuration, the developed probe exhibits fluorescence behavior. This probe was employed for sensing quercetin, with Cu^{2+} ions chosen as a quenching agent (Figures 8 A and B). In this scenario, the fluorescence property of the RP-GQDs@Zn-MOFs probe was observed to decrease (Turn-Off) upon the addition of Cu^{2+} ions, likely due to the formation of a complex between Cu^{2+} ions and RP-GQDs@Zn-MOFs (Cu^{2+}-RP-GQDs@Zn-MOFs). Subsequently, the introduction of quercetin led to the restoration of fluorescence in the Cu^{2+}-RP-GQDs@Zn-MOFs complex (Figures 8 C and D), indicating a proportional relationship between quercetin concentration and the recovered probe fluorescence (referred to as "Turn-On"). This provided a linear concentration range of 100 ng/mL to 1400 ng/mL ($Y = 4.2x + 777.8$, $R^2 = 0.99$). Additionally, the LOD and LOQ were determined to be 37.8 ng/mL and 114.7 ng/mL, respectively. Table 1 summarizes various types of sensors for the detection of quercetin. In summary, the utilization of sulfur-doped GQDs as a fluorescent sensor for the detection of quercetin requires a thorough discussion of sensitivity and selectivity.[22] The development of modern electrodes is essential for designing electrochemical sensors, and it is equally important to thoroughly discuss the selectivity study for quercetin. Additionally, a comprehensive exploration of the impact of current/voltage is necessary.[33,34] Similarly, the importance of selecting modified MOFs[35] as well as the use of carbon nanoparticles[36] should not be understated. However, it's crucial to note that the discussion should include specific details about their impact on selectivity and sensitivity analysis for quercetin detection. In the present work, it is confirmed that the designed nanoprobe offers a wide linear range and a low LOD. Interestingly, due to the coordination of quercetin with its 3-OH functionality (B ring) and 4-carbonyl groups (B ring) with Cu^{2+} ions, the addition of quercetin demonstrates signifi-

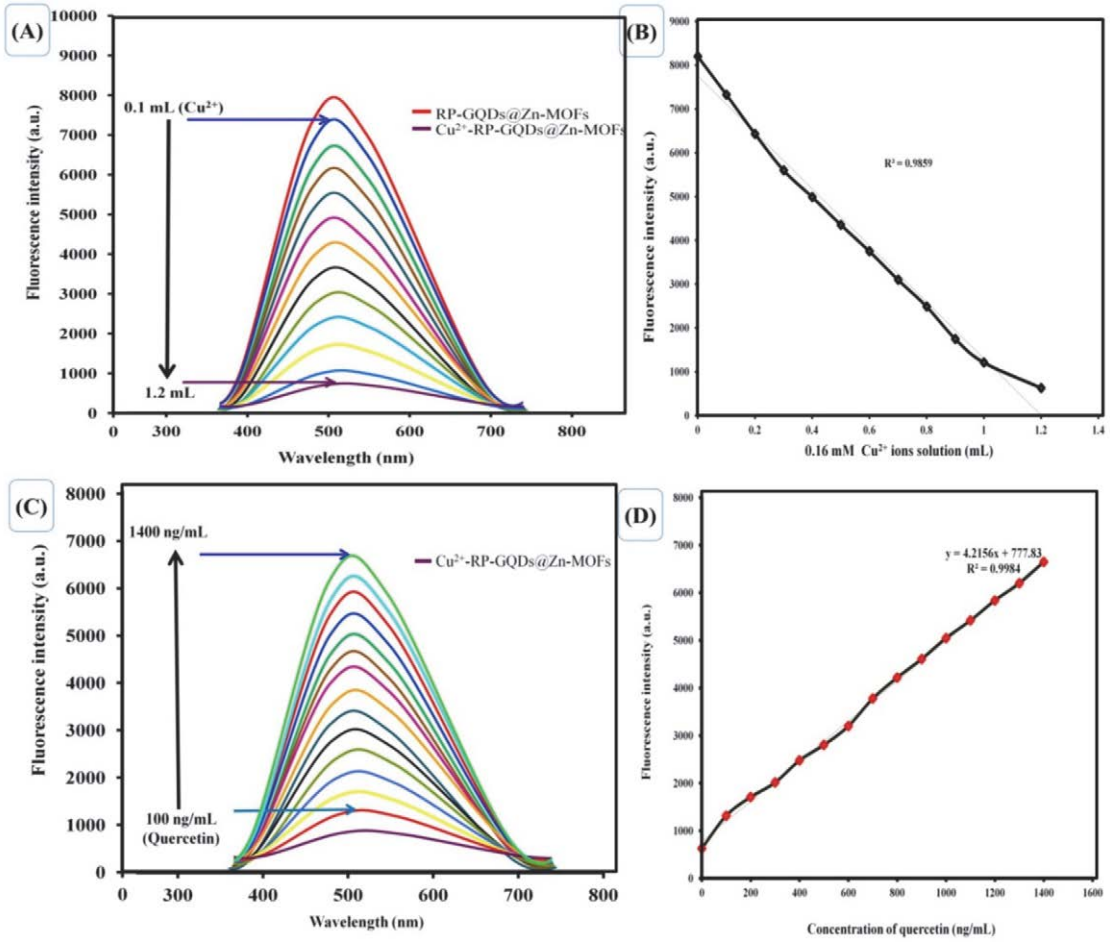

Figure 8: (A) Depicts the fluorescence quenching spectra of RP-GQDs@Zn-MOFs in the presence of Cu^{2+} ions. (B) Presents a graphical representation of the quenched fluorescence of the RP-GQDs@Zn-MOFs probe plotted against the concentration of Cu^{2+} ions. (C) Shows the fluorescence spectra of the Cu^{2+}-RP-GQDs@Zn-MOFs probe with varying concentrations of quercetin (ranging from 100 ng/mL to 1400 ng/mL). (D) Provides a graphical representation illustrating the relationship between quercetin concentration and the recovered fluorescence of the RP-GQDs@Zn-MOFs probe.

cant selectivity towards Cu^{2+} ions. In this context, 3-OH, with its more acidic proton, and 4-carbonyl groups are the preferred sites for complex formation. On the other hand, the 'C' ring, which contains 3'-OH and 4'-OH functionality, serves as the second site for complex formation. Additionally, the steric barrier of the first choice complex, combined with the lower proton acidity of 5-OH functionality, makes them non-reactive sites in quercetin sensing. Figure 9A illustrates the detection of quercetin using RP-GQDs@Zn-MOFs, followed by the formation of a Cu^{2+}-quercetin complex. Altogether, the proposed RP-GQDs@Zn-MOFs-based fluorescence probe, which exhibits a "Turn-On-Off-On" behavior, was found to be highly responsive to quercetin. The stability and reproducibility of the fluorescent RP-GQDs@Zn-MOFs probe were subsequently evaluated. In terms of stability testing, the %RSD was found to

Table 1: The summary of different types of sensors reported for detection of quercetin

Sr. No.	Type of sensor	Nanomaterial used	Linearity range	LOD	Ref.
1.	Fluorescent	Sulfur doped GQDs	0 to 50 µM	0.006 µg/mL	22
2.	Electrochemical	GQDs/Gold nanoparticle nanocomposite	0.01 to 6 µM	2 nM	33
3.	Amperometric	Aminated-GQDs/ thiolated β-cyclodextrin /gold nanoparticles	1 to 210 nM	285 pM	34
4.	Fluorescent	Carbon nanoparticles	3.3 to 41.2 µM	0.175 µM	36
5.	Fluorescent	MOFs	0.3 to 80 µM	0.14 µM	35
6.	Fluorescent	Cu^{2+}-RP-GQDs@Zn-MOFs	100 ng/mL to 1400 ng/mL	37.8 ng/mL	Present work

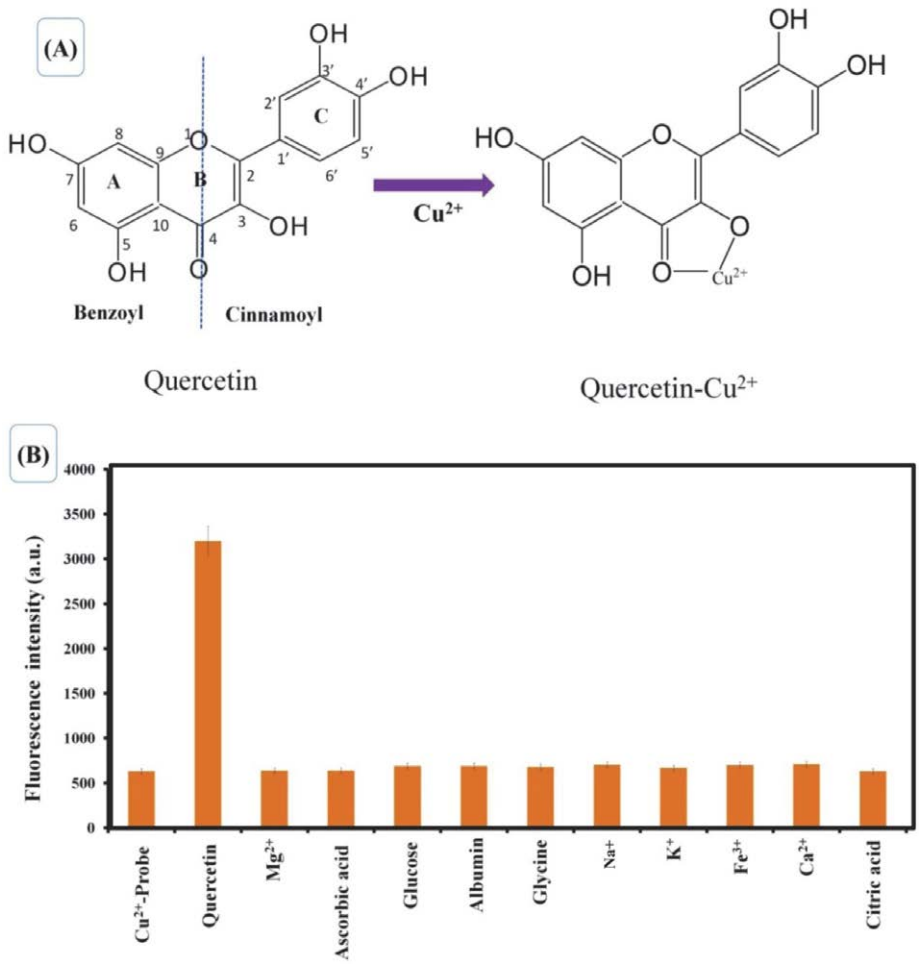

Figure 9: (A) Mechanism involved in quercetin detection using proposed design of RP-GQDs@Zn-MOFs nanoprobe and Cu^{2+} ions. (B) Interference study of RP-GQDs@Zn-MOFs fluorescence probe for detection of quercetin

be 1.3%, which is well below the 5% threshold, indicating that the probe remains robust under experimental conditions. Furthermore, repeatability testing yielded a %RSD of 1.8%, also meeting the criteria for reproducibility of the proposed sensor for quercetin measurement.

3. 8. Study of Selectivity and Real-Time Analysis

In this study, the selectivity of the RP-GQDs@Zn-MOFs fluorescence probe for quercetin was confirmed in the presence of various interfering compounds. Initially, the addition of copper ions to RP-GQDs@Zn-MOFs resulted in the formation of quenched Cu^{2+}-RP-GQDs@Zn-MOFs. Subsequently, the introduction of quercetin to this quenched Cu^{2+}-RP-GQDs@Zn-MOFs probe led to the recovery of fluorescence, thereby validating quercetin's exceptional selectivity even in the presence of multiple interfering compounds. Figure 9B illustrates the selectivity of quercetin amidst competing substances. The addition of various interfering agents to the quenched Cu^{2+}-RP-GQDs@Zn-MOFs probe resulted in the minimal recovery of quenched fluorescence compared to the control Cu^{2+}-RP-GQDs@Zn-MOFs quenched probe (absence of quercetin). This lack of significant recovery can be attributed to the absence of interactions between the Cu^{2+} ions (the quencher) responsible for quenching and the selected metal ions. Similarly, the use of citric acid, glycine, albumin, glucose, and ascorbic acid as interfering agents to assess the selectivity potential of Cu^{2+}-RP-GQDs@Zn-MOFs confirmed the high selectivity of the probe for quercetin alone. This selectivity is likely due to the specific interaction between copper ions and the 3-OH and 4-C=O functionalities of quercetin. Any minor changes in fluorescence recovery may be attributed to weak interactions between copper ions and amino acids, proteins, or other biomolecules, which have no significant impact on the selectivity of Cu^{2+}-RP-GQDs@Zn-MOFs. Additionally, the application of quercetin to simulated plasma samples resulted in a 97.42% recovery rate, with LOD and LOQ values of 38.11 ng/mL and 115.64 ng/mL, respectively. This demonstrates the feasibility of using the

Zn-MOFs@RP-GQDs probe for quercetin detection in complex samples. In the future, we intend to validate the RP-GQDs@Zn-MOFs-mediated fluorescence turn "On-Off-On" probe with preclinical blood samples as a proof of concept.

4. Conclusion

In this paper, we have presented an exceptionally stable and nanosized RP-GQDs@Zn-MOFs-based fluorescence turn "On-Off-On" nanoprobe. This innovative probe was developed by encapsulating RP-GQDs, synthesized from rose petals, within Zn-MOFs. The interaction between Zn^{2+} and carboxylic functionalities was employed to create RP-GQDs@Zn-MOFs, which was confirmed through spectroscopic analysis. Importantly, the encapsulation of RP-GQDs in Zn-MOFs retained the luminescent properties of RP-GQDs. The particle size analysis of the complex demonstrated the stability of Zn-MOFs. The study further showed that the presence of quercetin in the Cu^{2+}-RP-GQDs@Zn-MOFs sensing system led to fluorescence recovery. This recovery is attributed to the formation of a complex between Cu^{2+} ions and specific functionalities of quercetin, specifically the 3-OH and the carbonyl group (4-C=O) in the 'B' ring. This probe exhibited a low LOD of 37.8 ng/mL, indicating its high sensitivity for quercetin detection. Additionally, the probe's selectivity was assessed through interference testing, confirming its high specificity for quercetin in the presence of various interfering substances. The analytical parameters demonstrated the probe's stability and repeatability, making it a reliable sensing system for quercetin detection. Real-time analysis in artificial plasma validated its practical utility. In conclusion, the developed RP-GQDs@Zn-MOFs-based sensor offers a straightforward process, excellent sensitivity, and selectivity for quercetin detection. This sensor has the potential for applications in measuring quercetin levels in clinical samples and food products.

Conflict of interest

The author has declared that there are no conflicts of interest related to this research.

Acknowledgment

The researchers would like to extend their acknowledgments to the Principal of the H. R. Patel Institute of Pharmaceutical Education and Research in Shirpur for providing the essential research facilities. They would also like to express their appreciation to the Sophisticated Test and Instrumentation Centre in Cochin for granting access to HR-TEM analysis facilities. These acknowledgments highlight the importance of institutional support and collaboration in conducting successful research.

5. References

1. Y. Zhao, H. Zeng, X.-W. Zhu, W. Lu and D. Li, *Chem Soc Rev* **2021**, *50*, 4484–4513. **DOI:**10.1039/D0CS00955E
2. A. Mousavi, R. Zare-Dorabei and S. H. Mosavi, *Anal Methods* **2020**, *12*, 5397–5406. **DOI:**10.1039/D0AY01592J
3. G. L. Yang, X. L. Jiang, H. Xu and B. Zhao, *Small* **2021**, *17*, 2005327. **DOI:**10.1002/smll.202005327
4. S. N. Nangare, A. G. Patil, S. M. Chandankar and P. O. Patil, *J Nanostruc Chem* **2023**, *13*,197–242. **DOI:**10.1007/s40097-022-00479-0
5. G. Lu, S. Li, Z. Guo, O. K. Farha, B. G. Hauser, X. Qi, Y. Wang, X. Wang, S. Han and X. Liu, *Nature chemistry* **2012**, *4*, 310–316. **DOI:**10.1038/nchem.1272
6. Z. Li and H. C. Zeng, *Chem Mater* **2013**, *25*, 1761–1768. **DOI:**10.1021/cm400260g
7. S. N. Nangare, P. M. Sangale, A. G. Patil, S. H. Boddu, P. K. Deshmukh, N. R. Jadhav, R. S. Tade, D. R. Patil, A. Pandey and S. Mutalik, *Microchem J* **2021**, *169*, 106567. **DOI:**10.1016/j.microc.2021.106567
8. Y. Tao, Y. Jiang, Y. Huang, J. Liu, P. Zhang, X. Chen, Y. Fan, L. Wang and J. Xu, *CrystEngComm* **2021**, *23*, 4038–4049. **DOI:**10.1039/D1CE00392E
9. C. Yao, Y. Xu and Z. Xia, *J Mater Chem C* **2018**, *6*, 4396–4399. **DOI:**10.1039/C8TC01018H
10. H. Abdolmohammad-Zadeh and F. Ahmadian, *Microchem J* **2021**, *164*, 106001. **DOI:**10.1016/j.microc.2021.106001
11. G. Kaur, S. Sharma, S. Singh, N. Bhardwaj and A. Deep, *ACS Omega* **2022,** *7*,17600–17608. **DOI:**10.1021/acsomega.2c00126
12. X. Jiang, H. Jin, Y. Sun, Z. Sun and R. Gui, *Biosens Bioelectron* **2020**, *152*, 112012. **DOI:**10.1016/j.bios.2020.112012
13. J. Pantwalawalkar, S. Chandankar, R. Tade, Z. Khan, M. Shaikh, T. Powar, P. Patil, V. Sugandhi and S. Nangare, *Adv Nat Sci: Nanosci Nanotechnol* **2022**, *13*, 013001. **DOI:**10.1088/2043-6262/ac5e35
14. M. Li, T. Chen, J. J. Gooding and J. Liu, *ACS sensors* **2019**, *4*, 1732–1748. **DOI:**10.1021/acssensors.9b00514
15. R. S. Tade, S. N. Nangare, A. G. Patil, A. Pandey, P. K. Deshmukh, D. R. Patil, T. N. Agrawal, S. Mutalik, A. M. Patil and M. P. More, *Nanotechnology* **2020**, *31*, 292001. **DOI:**10.1088/1361-6528/ab803e
16. H. Sun, L. Wu, W. Wei and X. Qu, *Mater Today* **2013**, *16*, 433–442. **DOI:**10.1016/j.mattod.2013.10.020
17. R. S. Tade and P. O. Patil, *Curr Appl Phy* **2020**, *20*, 1226–1236. **DOI:**10.1016/j.cap.2020.08.006
18. R. Li, L. Liu, H. Zhu and Z. Li, *Anal Chim Acta* **2018**, *1008*, 38–47. **DOI:**10.1016/j.aca.2018.01.031
19. S. R. Ahmed, M. Sherazee, S. Srinivasan and A. R. Rajabzadeh, *Food Chem* **2022**, *379*, 132152. **DOI:**10.1016/j.foodchem.2022.132152
20. S. Nangare, S. Patil, S. Patil, Z. Khan, A. Patil and P. Patil, *Inorg Chem Commun* **2022**, *143*, 109751. **DOI:**10.1016/j.inoche.2022.109751
21. Y. Zou, F. Yan, T. Zheng, D. Shi, F. Sun, N. Yang and L. Chen, *Talanta* **2015**, *135*, 145–148.

DOI:10.1016/j.talanta.2014.12.029
22. S. Kadian and G. Manik, *Food Chem* **2020**, *317*, 126457. **DOI:**10.1016/j.foodchem.2020.126457
23. K. Ishii, T. Furuta and Y. Kasuya, *J Chromatogr B* **2003**, *794*, 49–56. **DOI:**10.1016/S1570-0232(03)00398-2
24. L. R. de Moura Ferraz, A. É. G. A. Tabosa, D. D. S. da Silva Nascimento, A. S. Ferreira, V. de Albuquerque Wanderley Sales, J. Y. R. Silva, S. A. Júnior, L. A. Rolim, J. J. de Souza Pereira and P. J. Rolim-Neto, *Sci Rep* **2020**, *10*, 1–14. **DOI:**10.1038/s41598-020-73848-w
25. H. Kaur, G. C. Mohanta, V. Gupta, D. Kukkar and S. Tyagi, *J Drug Deliv Sci Technol* **2017**, *41*, 106–112. **DOI:**10.1016/j.jddst.2017.07.004
26. M. Basiaga, Z. Paszenda, W. Walke, P. Karasiński and J. Marciniak: Information Technologies in Biomedicine, Volume 4, Springer, **2014**, pp. 411–420. **DOI**: 1007/978-3-319-06596-0_39
27. S. Zhu, Y. Song, X. Zhao, J. Shao, J. Zhang and B. Yang, *Nano Res* **2015**, *8*, 355–381. **DOI:**10.1007/s12274-014-0644-3
28. Y. Dong, J. Shao, C. Chen, H. Li, R. Wang, Y. Chi, X. Lin and G. Chen, *Carbon* **2012**, *50*, 4738–4743. **DOI:**10.1016/j.carbon.2012.06.002
29. D. Pan, L. Wang, Z. Li, B. Geng, C. Zhang, J. Zhan, L. Yin and L. Wang, *New J Chem* **2018**, *42*, 5083–5089. **DOI:**10.1039/C7NJ04909A
30. H. Yu, W. Zhu, H. Zhou, J. Liu, Z. Yang, X. Hu and A. Yuan, *RSC Adv* **2019**, *9*, 9577–9583. **DOI:**10.1039/C9RA01488H
31. Z. Tian, X. Yao, K. Ma, X. Niu, J. Grothe, Q. Xu, L. Liu, S. Kaskel and Y. Zhu, *ACS Omega* **2017**, *2*, 1249–1258. **DOI:**10.1021/acsomega.6b00385
32. X. Fu, H. Li, R. Lv, D. Hong, B. Yang, W. Gu and X. Liu, *J Solid State Chem* **2018**, *264*, 35–41. **DOI:**10.1016/j.jssc.2018.04.021
33. J. Li, J. Qu, R. Yang, L. Qu and P. de B. Harrington, *Electroanalysis* **2016**, *28*, 1322–1330. **DOI:**10.1002/elan.201500490
34. Z. Zhou, P. Zhao, C. Wang, P. Yang, Y. Xie and J. Fei, *Microchim Acta* **2020**, *187*, 1–9. **DOI:**10.1007/s00604-019-4106-1
35. P. Wu, Q. Du, L. Chen, M. Yang, Y. Sun, H. Zhi, P. Dramou and H. He, *Microchim Acta* **2021**, *188*, 1–8. **DOI:**10.1007/s00604-020-04664-2
36. P. Zuo, D. Xiao, M. Gao, J. Peng, R. Pan, Y. Xia and H. He, *Microchim Acta* **2014**, *181*, 1309–1316. **DOI:**10.1007/s00604-014-1236-3

Povzetek

Pričujoča študija predstavlja 'On-Off-On' nanoprobo na osnovi fluorescence kot možnost za zaznavanje kvercetina. Proba je narejena iz grafenskih kvantnih točk, proizvedenih iz vrtničnih cvetnih listov in vključenih v cinkova kovinsko-organska ogrodja (RP-GQDs@Zn-MOF). Z analizo velikosti delcev in HR-TEM smo potrdili sintezo uniformno porazdeljene probe v nanovelikosti, medtem ko je zeta potencial (+33,03 mV) dokazal njeno dobro stabilnost. Fluorescenčna analiza je potrdila, da dodatek bakrovih ionov (Cu^{2+}) povzroči dušenje fluorescence, medtem ko dodatek kvercetina povzroči nastanek kvercetin-Cu^{2+} kompleksa, kar privede do obnovitve zadušene fluorescence pri RP-GQDs@Zn-MOF zaradi statičnega dušenja. Nanoproba je izkazala široko koncentracijsko območje od 100 ng/mL do 1400 ng/mL (R^2 = 0,99) ter nizko mejo zaznave 37,8 ng/mL. Analiza selektivnosti je pokazala izrazito specifičnost za kvercetin, kar pripisujemo koordinaciji Cu^{2+} s karbonilnim kisikovim atomom in 3-OH skupino kvercetina. Nadalje je pripravljena proba pokazala odlično stabilnost, ponovljivost (RSD < 0,05) in potencial za analizo v realnem času.